Smart Materials and Structures

PURPOSE-LED PUBLISHING™

PAPER

IPMC as a mechanoelectric energy harvester: tailored properties

To cite this article: R Tiwari and K J Kim 2013 *Smart Mater. Struct.* **22** 015017

View the article online for updates and enhancements.

You may also like

- Characterizing the transduction behavior of ionic polymer-metal composite actuators and sensors via dimensional analysis
Zakai J Olsen and Kwang J Kim

- IPMC mechanoelectrical transduction: its scalability and optimization
D Pugal, P Solin, A Aabloo et al.

- The development of a method for crack-depth estimation in concrete by the electric response parameters to pulse mechanical excitation
T V Fursa, K Yu Osipov, B A Lukshin et al.

This content was downloaded from IP address 131.216.14.8 on 07/04/2026 at 18:57

Smart Mater. Struct. **22** (2013) 015017 (16pp) doi:10.1088/0964-1726/22/1/015017

IPMC as a mechanoelectric energy harvester: tailored properties

R Tiwari[1,2] **and K J Kim**[2,3]

[1] Dow Chemical Company, Midland, MI, 48667, USA
[2] Active Materials and Processing Laboratory, Department of Mechanical Engineering, University of Nevada, Reno, NV, 89557, USA
[3] Department of Mechanical Engineering, University of Nevada, Las Vegas, 4505 Maryland Parkway, Las Vegas, NV 89154, USA

E-mail: rtiwari@dow.com and kwang.kim@unlv.edu

Received 27 July 2012, in final form 20 November 2012
Published 17 December 2012
Online at stacks.iop.org/SMS/22/015017

Abstract
Due to their inherited mechanoelectric transduction capability, long-life, and effective operation in both air and water, ionic polymer–metal composites (IPMCs) are considered for energy harvesting applications. The reported research aims to study different parameters in the mechanical domain (stiffness and scalability) and the electrical domain (impedance and interfacial area) that seem to have profound effects on battery charging, with the aid of an electromechanical transducer model (Tiwari *et al* 2008 *Smart Struct. Syst.* **4** 549–3). Experiments performed to confirm the model predictions are also reported. The research demonstrates the applicability of IPMC as an energy harvester in lower frequency regions ($<$50 Hz) with an average efficiency of around 2% or less. The instantaneous power output from 10 mm (width) $\times$ 50 mm (length) $\times$ 0.2 mm (thickness) was measured to be approximately 4 μW (20 W m^{-3}).

(Some figures may appear in colour only in the online journal)

List of symbols

η_{bend}	Efficiency (%);
ρ''	Resistivity (Ω m);
C_n	Electrode capacitance (F);
f	Force (N);
f_R	Resonance frequency (Hz);
F_r	Frequency (Hz);
$2h/w$	Thickness/width (m);
i	Current (A);
κ_e	Dielectric permittivity (F m^{-1});
L_{free}/L_t	Free/total length of the sample (m);
M	Mechanical moment (N m);
N	Turn ratio of the transformer circuit (V N^{-1});
$P_{\text{out}}/P_{\text{in}}$	Output power/input power (W);
R_e	Intrinsic resistance of Nafion® (Ω);
R_n	Electrode resistance (Ω);
t	Time (s);
u	Tip displacement (m);
V	Output voltage (V);
Y	Young's modulus (Pa);
Z_e	Electrical impedance (Ω);
Z_m	Mechanical stiffness (N m^{-1})

1. Introduction

Due to the advancements in portable electronics and wireless technology, there is a growing need to tap into energy sources for uninterrupted operation of these devices. The wasted mechanical vibrations that are integral to many systems such as automobiles, ships, process instrumentation, aircraft, bridges, etc, have been considered for harvesting [2]. Vibration energy harvesters mainly comprise of a transducer with the mechanoelectric capability to convert mechanical vibrations to an electrical signal, a harvester circuit to condition the generated electrical signal into a useful form and a storage device like a battery and/or super-capacitor. Piezoelectric materials have been given great attention as vibration energy harvesters [2, 8, 74–76] in the frequency range above 100 Hz [3]. Often, however, the ambient

 © 2013 IOP Publishing Ltd Printed in the UK & the USA

source of vibration can fall in a lower frequency regime (1–10 Hz), although the expected power output could be relatively low compared to the high frequency regime. Hence, there is ample opportunity to develop low-frequency-vibration energy harvesters [77]. Due to their inherent flexibility, mechanoelectric coupling, ability to operate in both water [78] and air [4, 46, 79, 80], and long operating life, ionic polymer–metal composites (IPMCs) are excellent candidates for harvesting energy in the low frequency regime. A large amount of research has concentrated on the signal conditioning circuit, for optimal power output from the transducer [5–7] and storage devices [8]. However, IPMC as the transducer is less studied, and this is the main focus of this study.

Typically, IPMC is manufactured by sandwiching Nafion, a perfluorinated ionomer, between two metal electrode layers [9–11] and displays electromechanical and mechanoelectrical transduction. The electromechanical transduction occurs due to the motion of cations towards the cathode (cation-rich layer), along with water molecules, on application of an electric field (actuation voltage between 1–5 V). This causes the IPMC to swell near the cathode. The strain in the cation-rich layer induces extensional stresses in the polymer, resulting in a fast bending motion towards the anode [12]. The pressure from the strained polymer matrix causes water to diffuse out of the cation-rich area, resulting in a slow relaxation towards the cathode. A lifetime of 250 000 cycles was achieved in air operation when treated with ionic liquid [13]. The mechanoelectric transduction results from cation motion from the higher density region to the lower density region on mechanical deformation [14, 15]. An output in the range of 20–70 mV can be generated on mechanical deformation.

IPMCs are commonly employed in the bender configuration [16–20, 81, 82]. A variety of research has been performed on the four major aspects of IPMCs: fabrication, characterization, modeling and applications. Since the key role of the ionomers is charge transport, an attempt to improve the ionic conductivity has been made. Other properties that affect the transduction capabilities are the elastic modulus, ion exchange capacity and water uptake [21]. A number of models on understanding IPMC transduction have been reported in the literature [22–27]. Table 1 summarizes some of these key models that focus on the mechanoelectric transduction. IPMCs are being considered for applications like artificial muscle [28], robotic fish that can swim in water [29], aircraft wings [30], catheter tips [31], micro-robotics [32], automobiles and spacecraft [33] or stand-alone sensor–actuators for biomedical devices [34, 35].

Mechanoelectric transduction for energy harvesting using IPMC has been considered in the past. Martin [41] designed an energy harvester with a bandwidth 500 Hz with an expected power output of around 3 nW cm^{-2} at 4 Hz operating frequency. Brufau-Penella *et al* [42] developed a grey-box model to determine the optimal dimension of IPMC (length 12 cm and width 6.2 cm). At the optimal dimension IPMC generates 3 nW power when vibrated at 7.09 rad s^{-1} in air. Tiwari *et al* [1] demonstrated the harvesting capability of IPMC not only in bending but also in shear and tension. Under the optimal resistive load, the power outputs from platinum electroded IPMC of dimension 63 mm × 8.6 mm × 0.2 mm were measured to be 5 μW, 2.25 μW and 4.7 μW under bending, extension and shear loading conditions, respectively. Energy harvesting from base excitation in the fluid environment has also been reported [43]. The maximum power harvested was 1 nW for a base excitation of 1 mm. Aureli *et al* [44] also evaluated the energy harvesting capabilities of IPMC in a fluid environment. The power output from IPMC was observed to increase with frequency for a resistive load varying between 1 Ω and 1 MΩ. The maximum power at 10 Hz was measured to be around 1 nW mm^{-2} for an optimal load of 100 Ω. Giacomello *et al* [45] developed an underwater harvester based on flutter. The power output was measured to be around 1 nW for a resistive load of 10 kΩ and was observed to be dependent on the flapping frequency. Recently, energy harvesting from a three-dimensional IPMC disc has also been reported [46]. Farinholt *et al* [47] compared IPMC with PVDF (polyvinyl diflouride) under axial loading. Battery charging with PVDF was observed to be higher than with IPMC. IPMC was observed to be less efficient in comparison to PVDF under axial loading. This is due to the fact that IPMC is a natural bender.

Most of the reported work on energy harvesting using IPMC has focused on analyzing the basic energy harvesting capability or proof of concept. In addition, previous research has shown that the power generated from IPMC suffers from a low power density of around 1.2 μW kg^{-1}. No research has focused on enhancing the ways to improve the output of IPMC and hence battery charging; this paper aims to discuss different ways of doing so. There is also a need to analyze the efficiency of IPMC as an energy harvester in its natural bender configuration, which has not been considered previously.

This paper aims to evaluate various parameters that could impact the energy harvesting capability of IPMC. Since IPMC converts mechanical vibrations to an electrical signal, a transformer model is used for analyzing parameters that would have profound effects on the IPMC properties. Experiments to support the model predictions are also reported. The samples were directly tested under dynamic conditions, produced through programmed shaking, without the aid of a substrate.

2. The electromechanical transformer model

IPMC can be used as a mechanoelectric sensor by clamping it between two electrodes (figure 2). Electromechanical modeling helps in better understanding of the system and its response. This type of modeling, comprising of mechanical and electrical domains, can be represented by a transformer circuit, as shown in figure 1 [1, 48]. The applied mechanical force, f, and tip velocity, u', constitute mechanical domain parameters. The electrical domain consists of the electrical voltage, v, and current, i, produced by the IPMC. The model includes two impedance terms, Z_e and Z_m, in the electrical and mechanical domains, respectively. While the

Table 1. Comparison of some representative models developed to explain the mechanoelectric principle in IPMC.

Model	Reference	Description
Electrostatic model	[36]	Electrostatic forces were believed to play the dominant role. The mechanoelectric behavior was projected to be due to the different displacements of the effective charge centers of the anions and cations of each cluster.
	[17]	The model focuses on the electromechanical response based on cluster morphology and cation redistribution on application of an electric field. The hydration level and water migration were also incorporated. The model was used to study the electromechanical response of IPMC.
Grey-box model	[48]	A transformer-based equivalent circuit was developed to derive both the electromechanical and mechanoelectric responses of IPMC in a cantilever beam configuration. The coupling coefficients were derived using a pair of linearly coupled equations.
	[22, 26]	The model consisted of three key domains: electrical, stress generation and mechanical. The formulation was based upon experimental data.
Charge transport model	[37]	The internal charge dynamics was studied using one-dimensional linear partial differential equations.
	[56]	The model was based on the charge transport inside IPMC. The effect of distributed surface resistance due to porous electrodes was included.
Electrostatic polarization model	[38]	The model depicted the dominance of polarization in the mechanoelectric stage of IPMC. Forces on dipoles, pendant chain stiffness, cluster surface energy and external loading were taken into account.
Irreversible thermodynamic model	[39]	A linear irreversible thermodynamics based model was developed to formulate the mechanoelectrical and electromechanical behavior of IPMC.
Resistance model	[40]	The model illustrated the dependence of electrical parameters like the surface resistance on bending. The model was completely based on electrochemical analysis.
	[57]	A porous surface electrode was modeled to estimate the resistance and capacitance. Parameters like the electrode thickness and the porosity of the electrode were found to affect the resistivity whereas the interlayer electrode and the particle gap in that layer affected the capacitance.
	[83, 84]	Both surface and intermediate layer resistance were considered in the model. A physical phenomenological model that took into account three IPMC layers, surface electrode, intermediate composite and polymer layers, that was used for predicting mechanoelectrical behavior was developed.

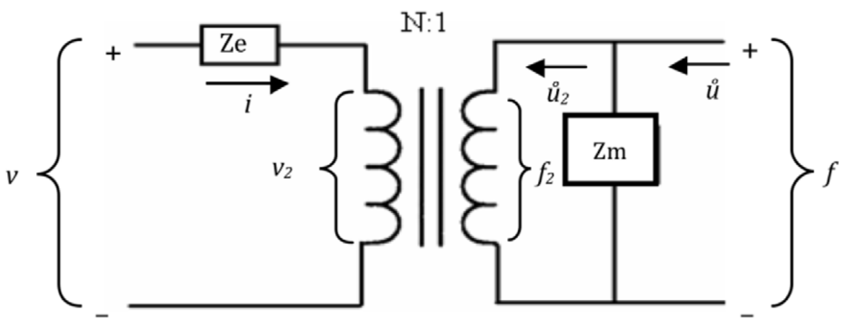

Figure 1. A transformer circuit to represent the electromechanical model of IPMC.

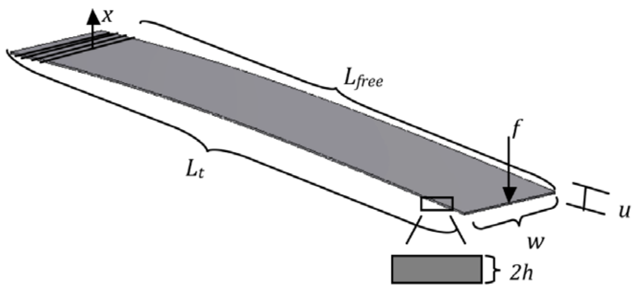

Figure 2. Mechanical specification of IPMC.

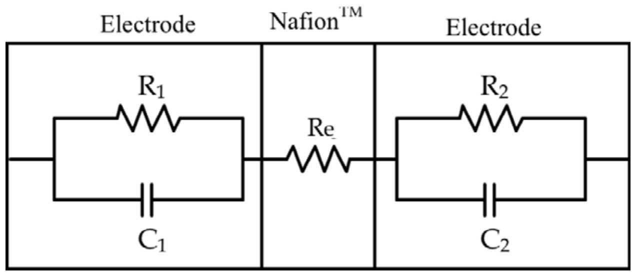

Figure 3. An equivalent RC circuit model.

electrical impedance is the result of the capacitive and resistive properties of IPMC, the mechanical impedance term represents its stiffness. For the purposes of simplicity it was assumed that the electrical and the mechanical domains were coupled linearly [48]. Figures 2 and 3 define the parameters in the mechanical and electrical domains.

Using the bender beam configuration and initial boundary conditions $(x = 0,\ \dot{u}(x) = 0)$ and $(x = 0,\ u(x) = 0)$ the mechanical impedance was calculated as [1, 48]

$$Z_m = \frac{1}{s}\frac{Y_W(2h)^3}{4L_{\mathrm{free}}^3}. \tag{1}$$

It has been shown that IPMC displays resistive behavior at low (0–10 Hz) and high frequencies (>100 Hz) [49]. At intermediate frequencies (10–100 Hz) it behaves like a capacitor. Since IPMC possesses both capacitive and resistive properties, it was modeled as an RC circuit [50], as shown in figure 3. Based on figure 3 the electrical impedance was formulated as

$$Z_c = \sum_{n=1}^{2}\frac{R_n}{R_nC_ns+1} + R_e, \qquad R_n = \frac{\rho''2h}{L_tw}, \qquad C_n = \frac{k_eL_tw}{2h}. \tag{2}$$

The transformer circuit previously shown in figure 1 has a turn ratio N which represents the electromechanical coupling. This turn ratio presents the relationship between the open-circuit voltage and the external force acting on the polymer and is derived as

$$N = \frac{3d_cL_{free}^2}{k_e^TL_tw2h}. \tag{3}$$

In equations (1)–(3), ρ_n is the resistivity and k_e is the permittivity of the IPMC sample. R_n and C_n are the resistive and capacitive components of the IPMC impedance, respectively. They are represented as R_1, R_2, C_1 and C_2 in figure 3. R_e is the intrinsic resistance of the base polymeric material, Nafion®. The capacitance of IPMC has been observed to decrease with frequency [51]. The measured capacitance varies from 10 to 20 mF cm^{-2} [51]. The governing equation for the coupling was derived as

$$\begin{Bmatrix} V \\ f \end{Bmatrix} = \begin{bmatrix} Z_e + Z_mN^2 & Z_mN \\ Z_mN & Z_m \end{bmatrix}\begin{Bmatrix} i \\ u' \end{Bmatrix}. \tag{4}$$

The mechanoelectric model is employed in the following section to predict battery charging using IPMC in the bender configuration. In addition, the effects of various factors, described in the model, on energy harvesting using IPMC are discussed. These include factors in the mechanical domain like the scalability (multilayer configuration and variable thickness) and in the electrical domain like the distributed surface impedance (electrode surface area and electrode thickness). The model provides a means to understand the effect of these parameters without involving complex physical phenomena.

It should be noted that the reported research not only aims to analyze the energy harvesting capabilities of IPMC, but also provides a comprehensive parametric study of the effects of different mechanical and electrical domain parameters that affect IPMC. These effects are not only studied through the electromechanical transformer model but also through experiments.

3. Factors affecting energy harvesting using IPMC

The electromechanical transformer model predicts that various parameters in the mechanical and electrical domains could have effects on IPMC's transduction properties. This is evident from equation (4). The turn ratio, N, of the transformer circuit, which defines the coupling between the electrical and mechanical domains, affects the voltage output in the open circuit. The turn ratio itself is affected by parameters in both domains. Hence, it is prudent to study the effects of these parameters individually. However, it should be noted that some of these parameters (especially the electrical impedance) cannot be isolated and may cause effects on other electrical domain parameters. Experiments were also performed to confirm the model predictions.

Ionic polymer–metal composite manufactured through electroless deposition exhibits distinct electrode, intermediate and polymer layers. It must be noted that the IPMC's properties are affected by the physics of each layer and the coupling between them. However, the electromechanical transformer model does not account for the ion transport inside the material.

3.1. Experimental set-up

For the energy harvesting experiments, a shaker assembly (TIRA Vibration System, TV52110) was used as the source of mechanical input. The shaker was programmed using

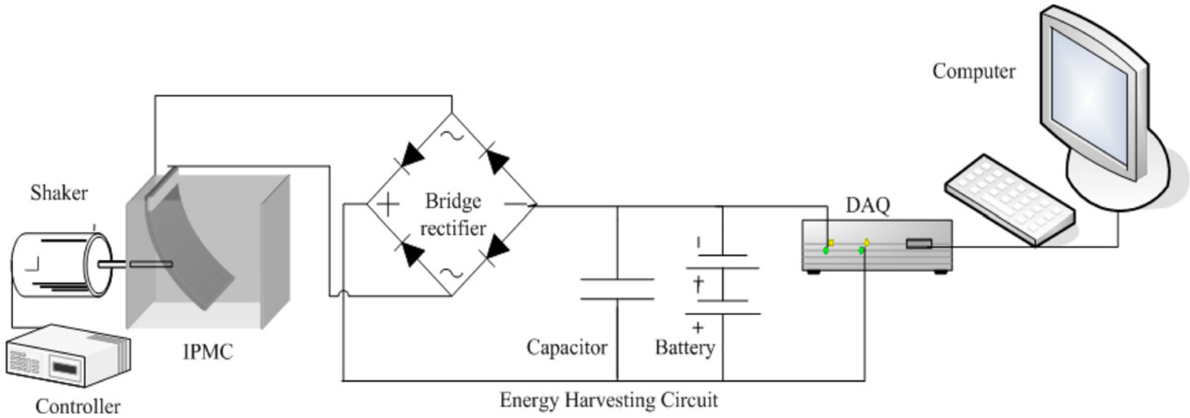

Figure 4. The energy harvesting set-up consisting of IPMC as the transducer, a full bridge rectifier circuit and NiMH as the storage device.

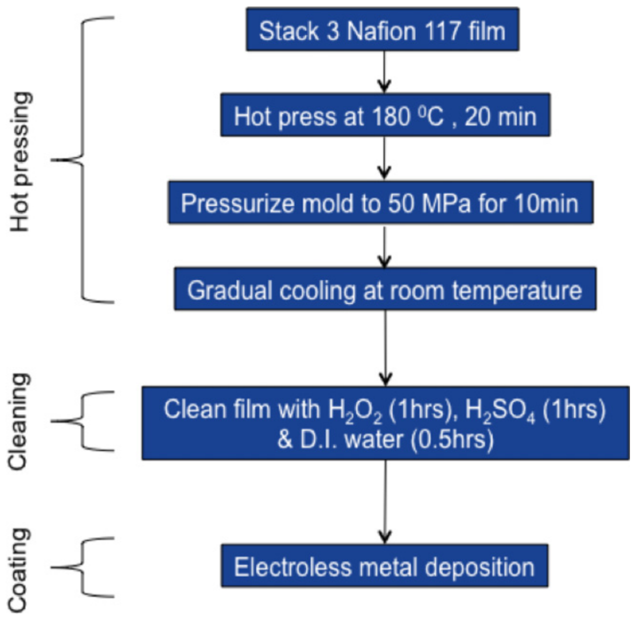

Figure 5. The manufacture of thicker IPMC using the hot-press method.

a VR8500 controller to produce a sinusoidal mechanical vibration at a frequency of 10 Hz. The shaft displacement was controlled at 0.5 inch (pk–pk). One end of the sample was clamped while the other end was pinned to the shaker shaft to have a better control on the sample bending. The experimental set-up is illustrated in figure 4.

Under dynamic excitation, the IPMC produced a sinusoidal waveform. This signal was rectified using a full bridge rectifier along with a 1000 μF capacitor connected across the output pins. Various rectifier circuits discussed previously [52, 53] were considered for minimizing the signal loss. However, these losses are integral to existing energy harvesting circuits and cannot be avoided. Since it is important to store the harvested energy for use when needed, the DC signal was used to charge a 40 mAh rechargeable NiMH battery (VARTA). The battery voltage was recorded using an IOTech Personal Daq 56 data acquisition system. IPMC samples were manufactured using the electroless deposition process [54] with platinum electrodes and Nafion 117. The sample length and width were 50 mm and 10 mm respectively.

In order to characterize the manufactured IPMC samples, scanning electron microscopy (SEM) was performed using a Hitachi S-4700. Cyclic voltammetry and impedance measurements were performed using the universal electrochemical laboratory system with a 20 A booster (VoltaLab80 PGZ402). The voltage was scanned from −1 to 1 V with a scan rate of 10 mVs^{-1} to obtain the voltammetry. On the other hand, the voltage was fixed at 1 V with 1 mV steps for the EIS (electrochemical impedance spectroscopy). The frequency was scanned between 100 mHz and 100 Hz.

The tensile modulus was measured using a universal testing machine (Instron 5565, USA). The fabricated IPMC samples were punched out using a dog-bone shaped punch mold followed by ASTM 638 and 882 and excess water on the surface was removed by pressing them on tissue paper before the experiments. The strain was applied at a rate of 10 mm min^{-1}. Any variations of the aforementioned set-ups will be specified in the following.

3.2. Mechanical domain parameters

3.2.1. Scalability. The effects of IPMC dimensions have been studied previously [1]. It was shown that change in the thickness of the sample has a more profound effect on the material output. In the following section, the effect of thickness was further investigated by manufacturing thicker IPMC using the hot-press technique.

3.2.1.1. IPMC thickness. The typical thickness of IPMC (0.2 mm) is limited by the commercial availability of base polymer membranes. In order to investigate the effect of thickness on battery charging, IPMC samples with a thickness of 0.5 mm were manufactured from Nafion 117 with the hot-press technique described in figure 5. The membrane was cut into the required dimensions and stacked into a mold covered with Teflon film. For the purposes of the experiment three Nafion films were used. The cleaned thicker Nafion film hence produced was coated with metal using electroless deposition. The length and width were 25 mm and 12.5 mm, respectively.

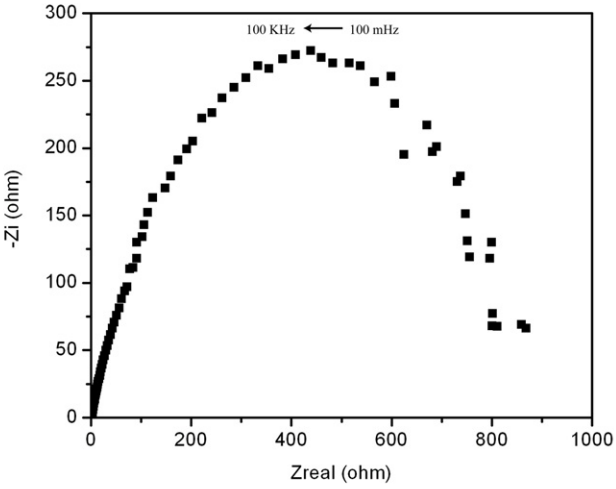

Figure 6. The result of electrochemical analysis: EIS in 1 M H_2SO_4 solution.

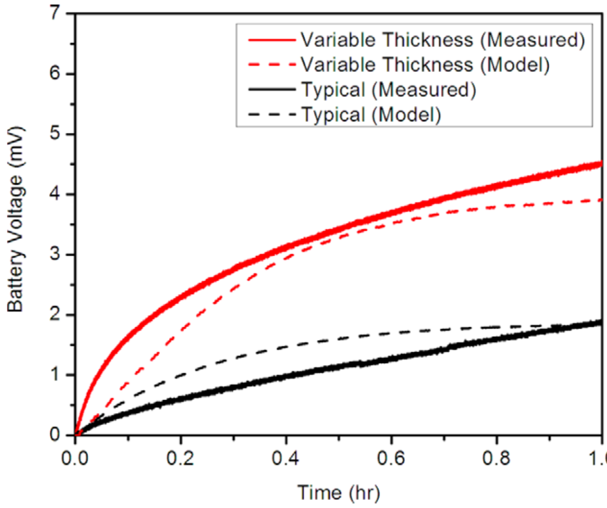

Figure 8. Battery charging using the increased thickness IPMC.

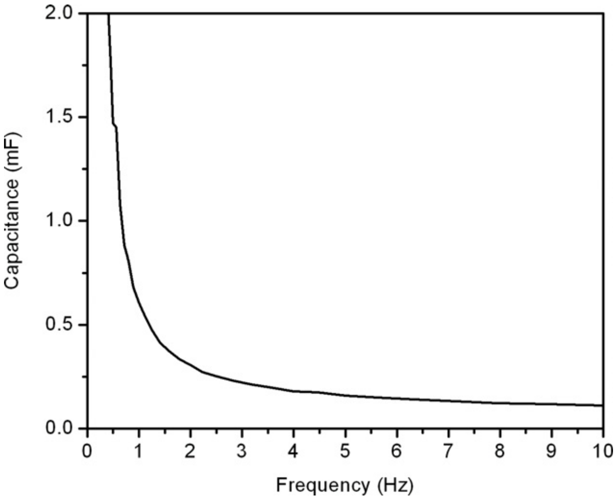

Figure 7. Capacitance measurement in 1 M H_2SO_4 solution.

The impedance was measured using a potentiostat with a three-electrode system in 1 M H_2SO_4. The frequency range was from 100 kHz to 100 mHz. The results of the electrochemical test are shown in figures 6 and 7. The impedance curve is a representative characteristic of the RC circuit of the electrical component in the electromechanical model. Based on the EIS data it can be concluded that the capacitance of variable thickness IPMC is around 25 mF, which is slightly higher than that of typical IPMC (20 mF). Due to the increased thickness, the dielectric property of the material becomes apparent as compared to typical IPMC of the same dimensions, thus leading to an increase in overall capacitance. Increasing the thickness also increases the stiffness of the sample.

An energy harvesting experiment was performed with an angular displacement of 11.4° for both the typical and the variable thickness IPMC. Both the anticipated and the measured charging of the battery are given in figure 8. As expected, the battery charging achieved using variable thickness IPMC was 4.5 mV after 1 h of charging. This is nearly twice as much as that achieved by a typical IPMC. As mentioned before, increasing the thickness of the IPMC led to an increase in the capacitance. Due to the increase in the capacitance, the rate of charging with thicker IPMC was measured to be lower than that for a typical IPMC sample (figure 8).

3.2.2. Multilayer IPMC. As the output from a single IPMC sample is low, the output from various samples could be combined to improve battery charging. Two combination techniques were used to manufacture multilayer IPMCs from individual layers: serial and parallel; both of these techniques involved IPMC in the standard beam configuration. Two layers were employed for each configuration. It was assumed that the IPMC samples shared the same electrical characteristics. Each layer was 30 mm in length and 10 mm in width with a thickness of 0.2 mm.

The serial multilayer configuration (SMC) was developed by stacking IPMC samples on top of each other, with the electrode connection shown in figure 9(a). The voltage was measured across the stack.

If n_L is the total number of layers in the SMC and v is the voltage measured, then

$$V_j \frac{V}{n}, \qquad j = 1 \ldots n_L. \tag{5}$$

The parallel multilayer configuration (PMC) was achieved by stacking IPMC samples on top of each other with a thin insulator layer in between and the electrical connection shown in figure 9(b). The voltage was measured across the stack as in the case of the SMC.

On the other hand, the voltage in each layer of the PMC is

$$V_j = V, \qquad j = 1 \ldots n_L. \tag{6}$$

In order to simulate the battery charging, equation (4) was rewritten for the multilayer configurations (SMC and PMC). The mechanical, electrical and coupling were modified as follows.

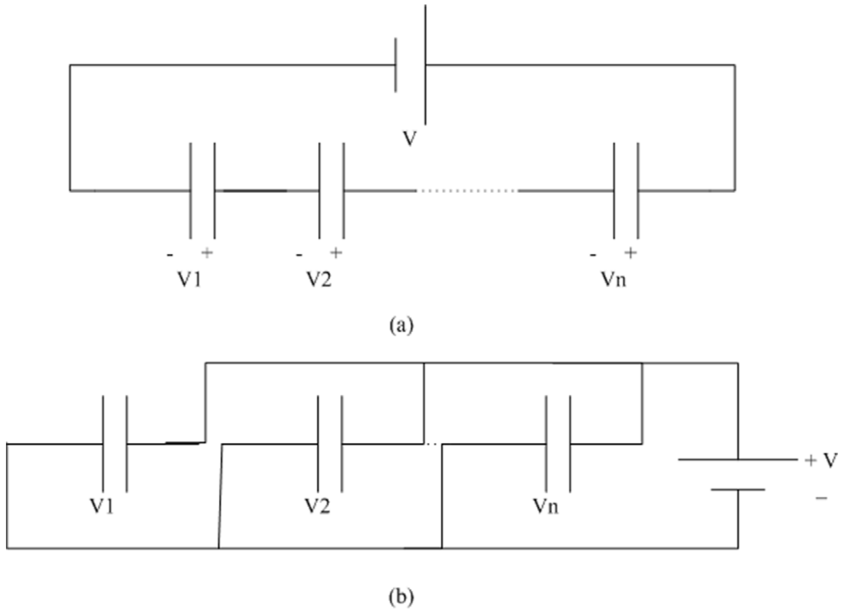

Figure 9. The serial multilayer configuration (a) and the parallel multilayer configuration (b) of the IPMC.

Let n_L be the number of layers in the multilayer stack. The total thickness of the multilayer stack is

$$h_L = n_L h. \tag{7}$$

Hence the mechanical component for the series and parallel configurations is given as

$$Z_{m\mathrm{MC}} = \frac{1}{s}\frac{Y_W(2h_L)^3}{4L_{\mathrm{free}}^3}. \tag{8}$$

The electrical impedances in the series and parallel configurations for the multilayer IPMC are

$$\begin{aligned} Z_{e\mathrm{SMC}} &= n_L Z_e, \\ Z_{e\mathrm{PMC}} &= \frac{Z_e}{n_L}. \end{aligned} \tag{9}$$

The velocity across each layer in the multilayer configurations remains constant. In order to relate the coupling to the voltage equation (3) was modified as

$$\begin{aligned} N_{\mathrm{SMC}} &= n_L N, \\ N_{\mathrm{PMC}} &= N. \end{aligned} \tag{10}$$

Thus, the modified mechanoelectric equation for multilayer IPMC in series and parallel configurations is

$$\text{series}: \quad \begin{Bmatrix} V \\ f \end{Bmatrix} \begin{bmatrix} n_L Z_e + n_L^5 Z_m N^2 & n_L^4 Z_m N \\ n_L^4 Z_m N & n_L^3 Z_m \end{bmatrix} \begin{Bmatrix} i \\ u' \end{Bmatrix}, \tag{11}$$

$$\text{parallel}: \quad \begin{Bmatrix} V \\ f \end{Bmatrix} \begin{bmatrix} \frac{Z_e}{n_L} + n_L^3 Z_m N^2 & n_L^3 Z_m N \\ n_L^3 Z_m N & n_L^3 Z_m \end{bmatrix} \begin{Bmatrix} i \\ u' \end{Bmatrix}. \tag{12}$$

The results of the energy harvesting experiment along with model predictions are shown in figure 10.

The battery charging was observed to be higher for the SMC. This could be because electrodes that are connected to each other act as low resistance paths for charge motion from one layer to another. The overall mechanical stiffness increased for the multilayer configurations. The coupling coefficient for the SMC increased linearly with the number of layers in the SMC. It should be noted that there is a limitation in controlling the IPMC impedance during manufacture, which may affect the total outputs of the multilayer configurations. Using layers cut from the same IPMC sample may reduce this error to some extent.

3.3. Electrical domain parameters

Ion transport inside the IPMC membrane on bending causes accumulation of charge on the electrode surface. The correlation between electrode properties and IPMC transduction has been previously reported [55–57]. Different metals like gold, silver, platinum, carbon and copper have been used in the past for fabricating IPMCs. Table 2 summarizes properties of IPMCs manufactured with different electrodes. From the table we can observe that the electrode metal and electrode deposition process (chemical deposition, sputter coating or plasma treatment) greatly affect the capacitance of the IPMC. This is because the particle size and its penetration along with the surface conductivity are dependent on the fabrication technique and pre-deposition surface treatment of the polymer.

The electromechanical transformer model incorporates the electrode properties in terms of impedance. Electrode properties such as the thickness, impedance and interfacial area between the electrode and the polymer are investigated in the reported study.

3.3.1. Electrode thickness. Electrodes deposited by sputter coating Nafion® with platinum were manufactured to better

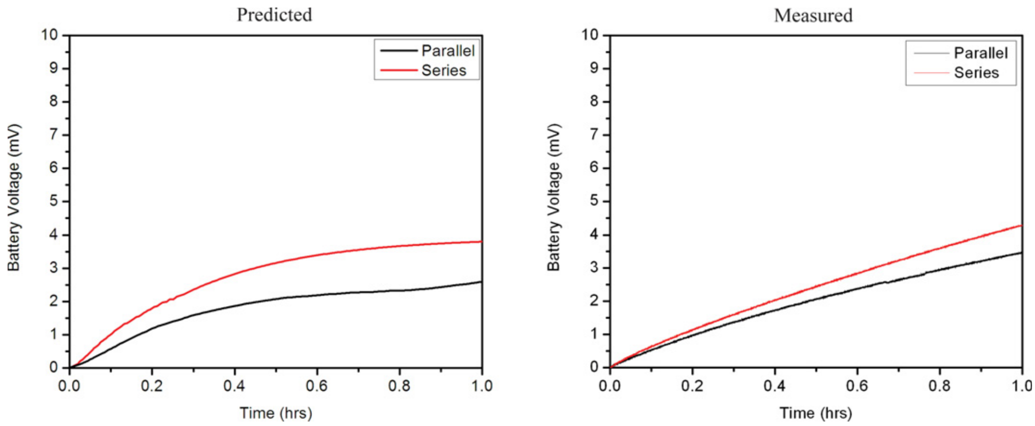

Figure 10. Energy harvesting using multilayer IPMC.

Table 2. Properties of IPMCs with different electrodes [68].

	Electrode thickness (μm)	Surface conductivity	Capacitance (μF cm^{-2})	Modulus (MPa)
Plasma-Pt	1.5–3	4 Ω/sq	1190	1100
Typical-Pt	4–15 [69]	1–4 Ω/sq	15–40	30–60
Pt–Au	1.4	1.3–3.8 Ω/sq		
Pt–Ag		0.4 Ω cm^{-1}		
Cu–Pt	2	6–11 Ω cm^{-1}		52.40
Au	1.4 [70]–7 [71]		1 mF [70]	70.9
Au flakes	0.270	1 Ω cm^{-1}		
Ni–Au [72]	10–25			
Carbon [73]	25	0.6 Ω cm^{-1}	16–51 mF	97–103
Cu		3–4 Ω cm^{-1}		
RuO_2 [73]	25	0.5 Ω cm^{-1}	20–36 m	88–95

understand the effect of electrode thickness on energy harvesting. Sputter coating restricts electrode deposition on the polymer surface eliminating metal dispersion inside the polymer membrane. Sputter coating was performed at 30 mA for three minutes per side per deposition using an EMITECH K575X machine. Impedance spectroscopy was performed to study the effect of increased electrode thickness on IPMC capacitance.

Electrodes coated through sputtering were observed to have smoother surfaces and hence low surface resistivities of 0.01 Ω/sq and 0.3 Ω/sq for one and two times sputter coated samples, respectively. The electrode thicknesses achieved by one and two times sputter coating were 30 μm and 45 μm, respectively as compared to 5 μm for typical IPMC. The sputter coated IPMC was observed to be stiffer and more susceptible to cracking. Due to an improvement in surface conductivity and material stiffness, the material showed higher battery charging (figure 11(c)). Due to the increased capacitance of the sputter coated samples (figures 11(a) and (b)) the rate of charging was measured to be lower than for a typical IPMC.

3.3.2. IPMC impedance. The IPMC impedance is the resultant of the electrode resistivity, the capacitance due to the metal particle dispersion inside the polymer membrane and the interfacial area between the electrode and the polymer. The effects of interfacial area and electrode properties on IPMC transduction have been investigated previously [58–60].

Surface roughening is typically performed to improve the electrode attachment on the polymer film. However, in the reported research polymer surface roughening was employed as a means to increase the interfacial area between the electrode and the polymer and hence modify the IPMC impedance. It was also believed that directional roughening and perforation would not only affect the interfacial area but also the electrode resistance and capacitance. IPMC samples were manufactured by roughening: (1) along the length of the IPMC, (2) cracks across the length of the IPMC (using sandpaper size 320) and (3) randomly perforating both sides of the Nafion using a needle with a tip diameter of 300 μm.

The effect of surface roughening was examined using SEM, as shown in figures 12 and 13. The figures show the cracks on the surface for samples 1 and 2. The SEM for sample 3 shows cracks in different directions whereas the cracks for samples 1 and 2 are more directional. Small numbers of cracks were also observed on a typical IPMC surface. These cracks are induced due to the sample handling. Directional roughening and perforation were also observed to impact the interfacial area and electrode roughness (figure 13). From figure 13 it can also be seen that the metal particle

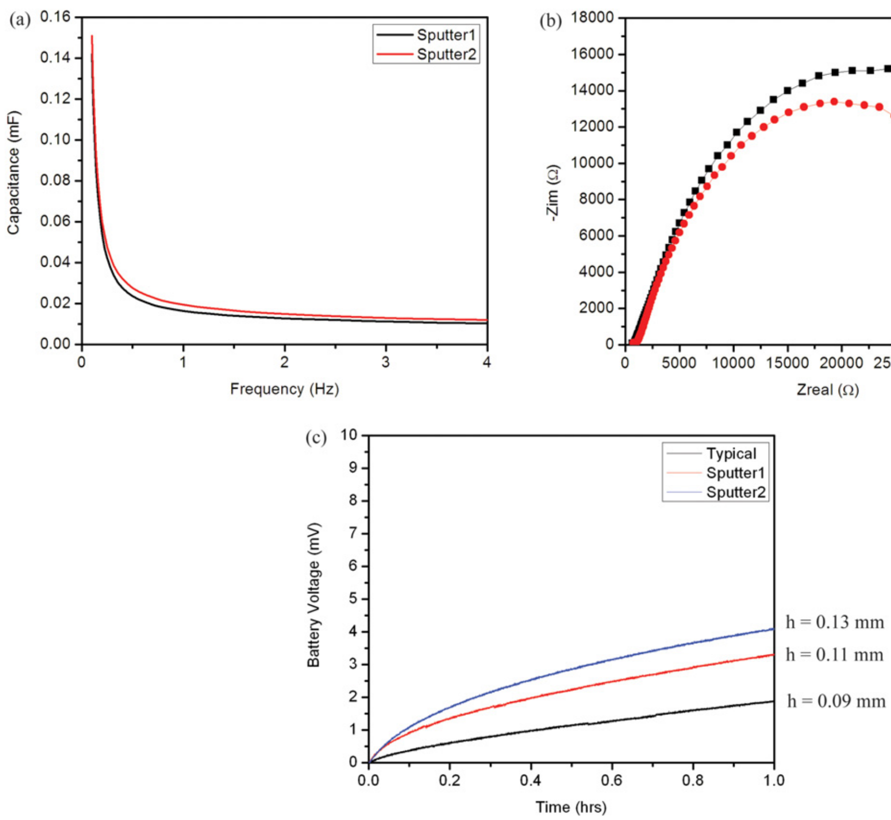

Figure 11. Surface capacitance measured using a conductivity cell (a), impedance spectroscopy (b) and battery charging (c) for sputter coated samples. 'Sputter1' and 'Sputter2' represent one and two times sputter coated samples.

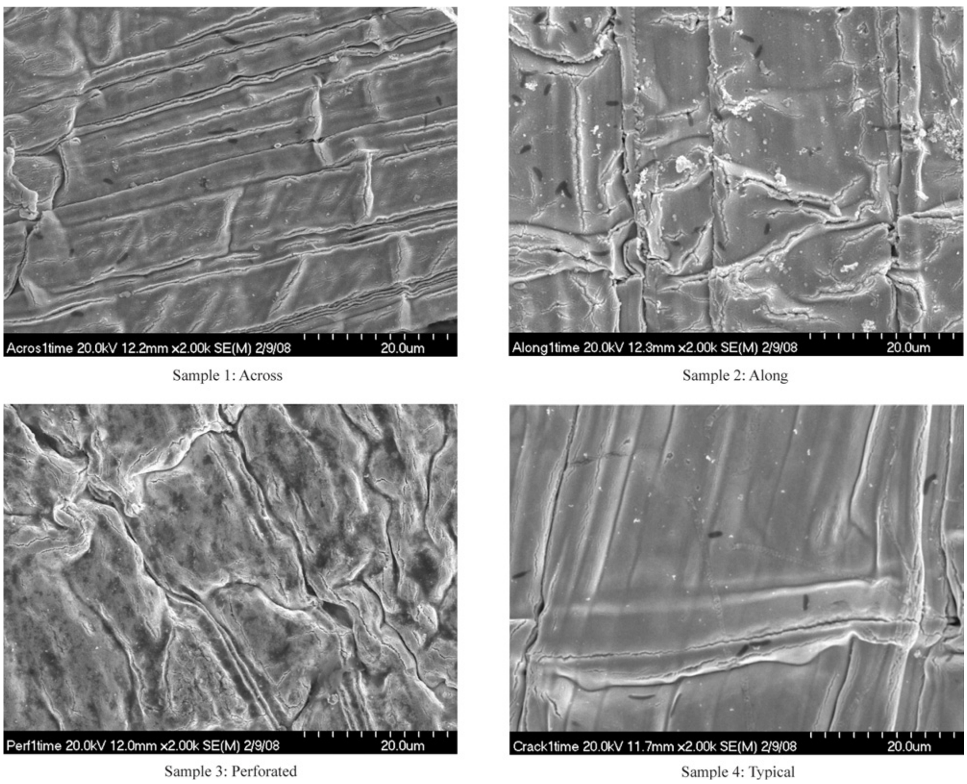

Figure 12. SEM showing the representative surface morphology of IPMC samples to study the distributed surface impedance [83].

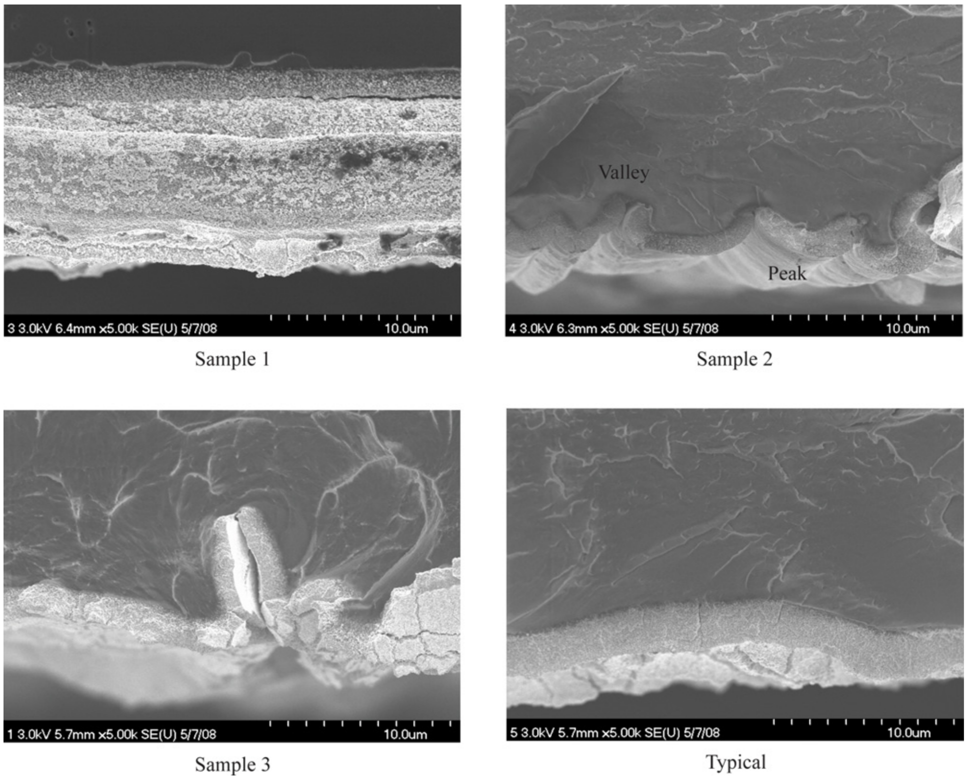

Figure 13. SEM micrographs of samples 1–3 and a typical IPMC sample after three-time reduction [83].

penetration inside the polymer was higher for sample 3. The effects of directional roughening and perforation were further studied using impedance spectroscopy. The real impedance values for different IPMC samples might shed some light on the resistance due to the interfacial layer. Poor harmony between the polymer membrane and the electrode can result in a higher impedance value. The higher value of this impedance leads to poor electromechanical properties and hence lowers the output from the IPMC. Figure 14(a) shows impedance spectroscopy for the different samples. The curves depict capacitive–resistive behavior. The impedance for sample 1 was higher than those for the other samples. This was believed to be due to the greater number of peaks and valleys formed due to the surface roughening, as shown in figure 13. The capacitance of the IPMC decreased with increase in frequency because the capacitance is inversely proportional to the frequency (figure 14(b)). This decrease with frequency was in accordance with the typical behavior of a capacitor. The capacitance value of sample 3 was higher than those in the other types of IPMC sample. This was believed to be caused by the higher electrode area as a result of perforation.

The electrodes might be affected by the charge on the surface. Hence cyclic voltammetry was performed using a three-electrode system. figure 14(c) compares cyclic voltammograms of IPMC samples after three-time reduction. No distinct electrochemistry was expected to occur between the scanning potentials of -1 and 1 V. As the signal generated by IPMC falls in the low voltage range we believe that it did not lead to oxidation–reduction on the electrode surface causing electrode degradation. The *I*–*V* curve in figure 14(c) also illustrates that sample 3 did not show any significant hysteresis. On the other hand, sample 1 showed the greatest hysteresis, followed by sample 2 and the typical IPMC, in that order. In another set of experiments the tensile moduli of the IPMC samples were measured. Care was taken to keep the samples hydrated during the experiment. As shown in figure 15, sample 3 showed the highest modulus, followed by samples 1 and 2. The typical IPMC demonstrated lowest modulus. According to the law of mixtures, the IPMC stiffness is the resultant of the polymer stiffness and the electrode stiffness. Platinum reduction inside the IPMC could have caused the increase in modulus in the case of sample 3. The results of the above experiments are summarized in table 3. An improvement in the mechanoelectric properties of sample 3 was observed based on the experimental results.

In order to verify the hypothesis that a reduction in surface impedance leads to an improvement in battery charging the samples were vibrated using the shaker assembly. The result is shown in figure 16(a) and compared with the predicted charging using the electromechanical transformer model (figure 16(b)). It is believed that sample 3 showed an improvement in battery charging due to an increase in the surface area of the electrode. Perforation causes the metal particles to penetrate further inside the membrane leading to an increase in the interfacial area between the electrode and the polymer. An increase in the surface area can also be confirmed based on an increase in the capacitance of the IPMC sample. Since perforation only has an effect on the interfacial area, the surface resistivity of sample 3 was almost the same as for a typical IPMC sample, as summarized in

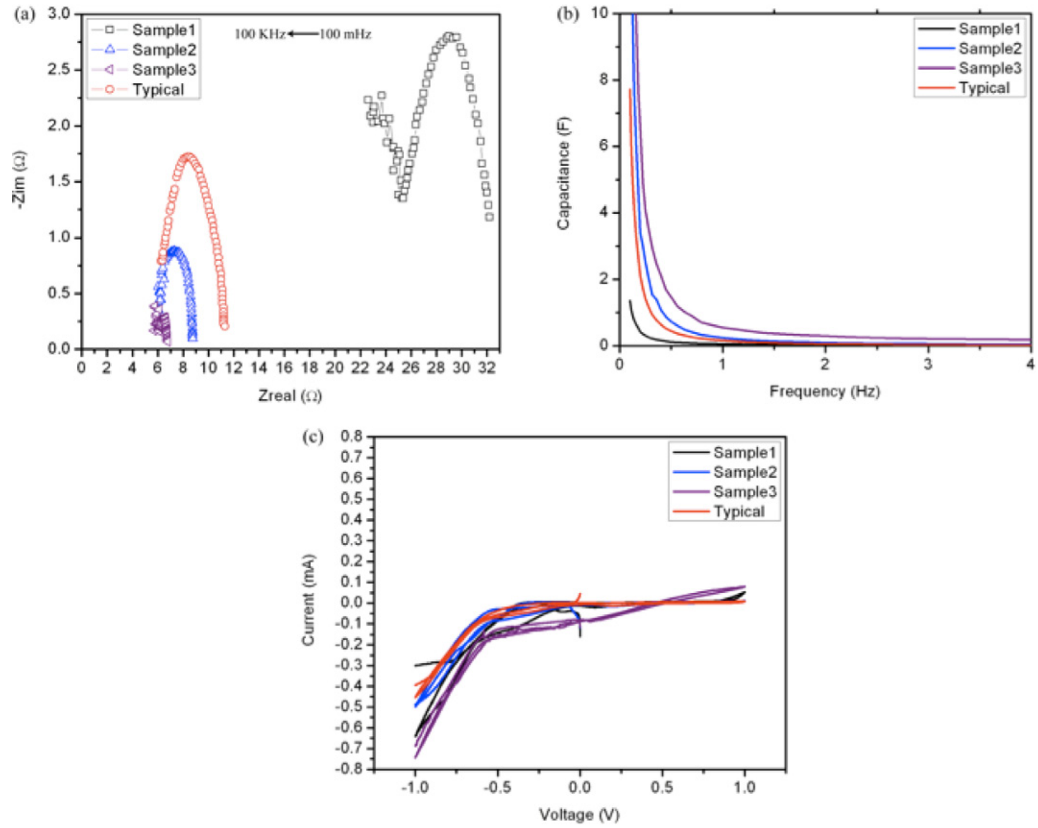

Figure 14. Impedance spectroscopy (a), capacitance (b) and voltammogram (c) of IPMC samples after three-time electroless deposition. The size of the samples was 10 mm × 50 mm × 0.20 mm [83].

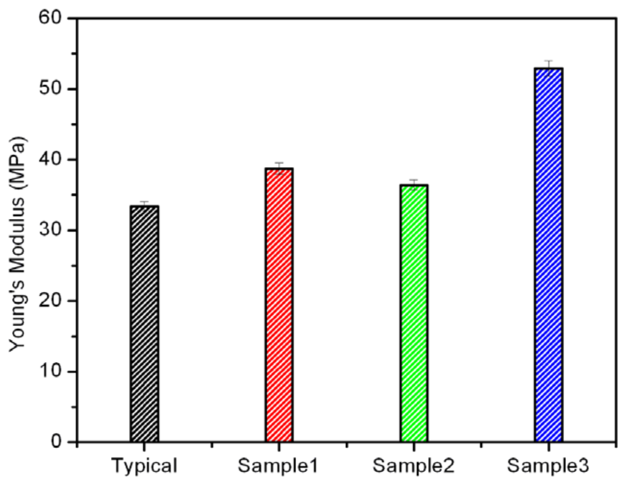

Figure 15. Young's moduli for the different samples, data taken from [83].

table 3. As seen from the SEM for each sample, directional roughening has an effect on electrode roughness and hence electrode impedance.

4. Power output/efficiency of a typical IPMC

It is important to determine the power generated by an IPMC to identify its feasibility for engineering applications. Experiments were conducted to determine the optimal resistive loads for both platinum and gold electroded IPMC samples in the bending mode (figure 17). The instantaneous power, P_{bend}, calculated by measuring the voltage drop, V, across the load resistance, R, is

$$P_{bend} = \frac{V^2}{R}. \tag{13}$$

It is evident from the graph that the platinum electroded sample produced slightly more power than the gold electroded sample. The optimal resistive load for maximum power dissipation was experimentally evaluated to be 38 KΩ for both the samples.

The efficiencies of three IPMC samples with platinum electrodes were individually measured [63] to determine the effectiveness of IPMC as an energy harvester,

$$\eta_{bend} = \frac{P_{out}}{P_{in}} \times 100$$
$$= \frac{1}{m}\sum_{n=2}^{m} \frac{\frac{(V_n - V_{n-1})^2}{R}}{\frac{[(f_n - f_{n-1})\cdot(u_n - u_{n-1})]}{(t_n - t_{n-1})}} \times 100, \tag{14}$$

where η_{bend} is the efficiency in the bender configuration, V is the voltage drop across resistance R, t is the time increment between data points, n is the sampled data and m is the total number of data points. Using the above equation the efficiency was calculated for three typical IPMC samples. Figure 18

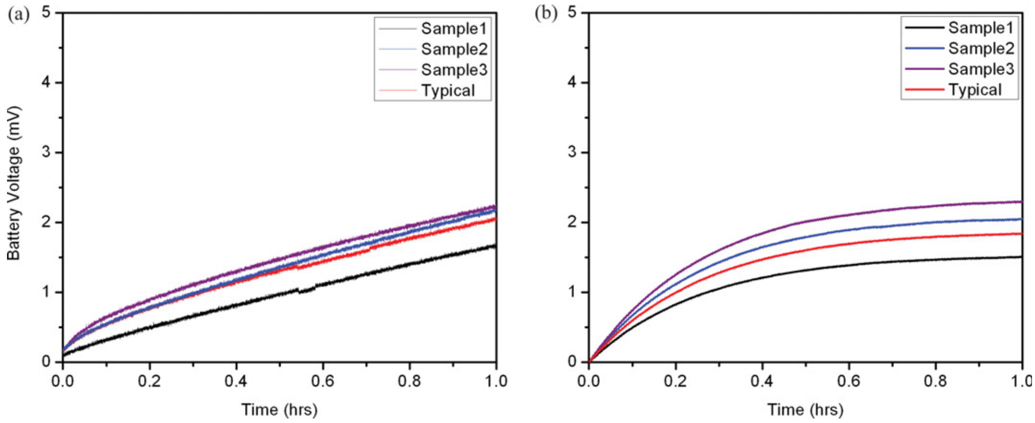

Figure 16. Voltage on the battery as measured (a) [83] and predicted (b) using different samples with modified surface impedances.

Table 3. A summary of the properties of the IPMC samples with different surface impedances.

Property	Sample 1	Sample 2	Sample 3	Typical	Literature
Average resistivity (Ω/sq)	13.50	17.50	7.96	8.22	1–4 [61, 62]
Average hysteresis (I–V curve)	High	Moderate	Very low	Low	Low
Average capacitance @ 10 Hz (mF cm^{-2})	∼4	∼10	∼34	∼6	2.48 [61]
Average Young's modulus (MPa)	38.0	36.0	52.5	33.5	30–60 [51]

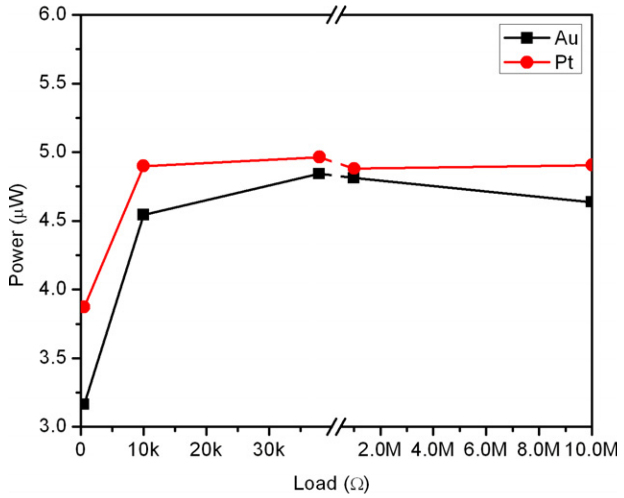

Figure 17. Output power as a function of resistive load measured experimentally in the bending mode.

Table 4. Energy efficiencies calculated for different IPMC samples.

Sample	Calculated efficiency (%)
1	1.73
2	1.40
3	1.89

shows the applied tip displacement, the force at the base of the sample and the voltage generated by the samples under consideration with the corresponding efficiencies in table 4.

The efficiency was observed to vary between 1% and 2%. Figure 18(d) shows the measured efficiencies at different frequencies of operation. The amplitude of the input vibration was controlled at 0.5 in (pk–pk) using a shaker. The frequency was varied between 1 and 40 Hz. An efficiency of 1.7% was measured at 10 Hz. Figure 19 lists the available technologies along with frequencies of vibration and the outputs generated from them [64]. Figure 20 compares the power densities produced by IPMC with other energy harvesting technologies including piezoelectric and solar [65]. The power densities and the frequencies of operation of various vibration-based energy harvesters reported in the literature and available on the market are plotted in figure 21. As can be seen from the figure, IPMC produced less power density as compared to other technologies like solar and thermoelectric, with an efficiency comparable to that of piezoelectric material.

Table 5 compares IPMC with PZT and PVDF as potential energy harvesters in the bending mode. The efficiency calculated for the PZT sample (using the above method) as reported in the literature [8] when vibrated at the resonance frequency was calculated to be around 5%. On vibration using a chirp signal with a frequency between 0 and 500 Hz the efficiency reduced to around 3%, while on using a random signal (0–500 Hz) the efficiency increased to approximately 7%. PZT bimorphs designed for energy harvesting have shown efficiencies of around 1% [66].

The low value of the electromechanical coupling coefficient of IPMC imposes a limitation on its efficiency. In addition, the coefficient 'd_c' for IPMC is dependent on the sample dimensions and is not represented as an intrinsic property. Further research is required in order to intrinsically measure the overall coupling coefficient.

Similarly to piezoelectric materials, IPMC stores generated energy inside itself. Thus by reducing the amount of

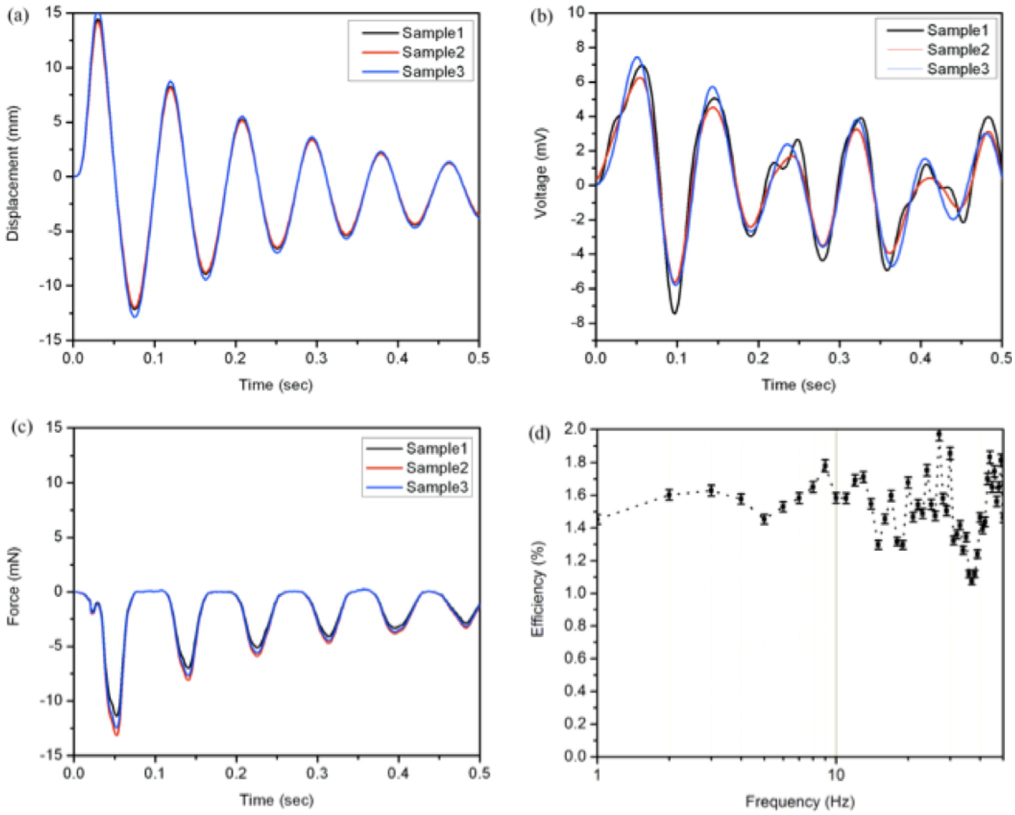

Figure 18. Measured tip displacement (a), applied force (b), output voltage measured (c) and average efficiency at different frequencies with 0.5 in (pk–pk) amplitude (d) using three 10 mm × 50 mm × 0.2 mm IPMC samples.

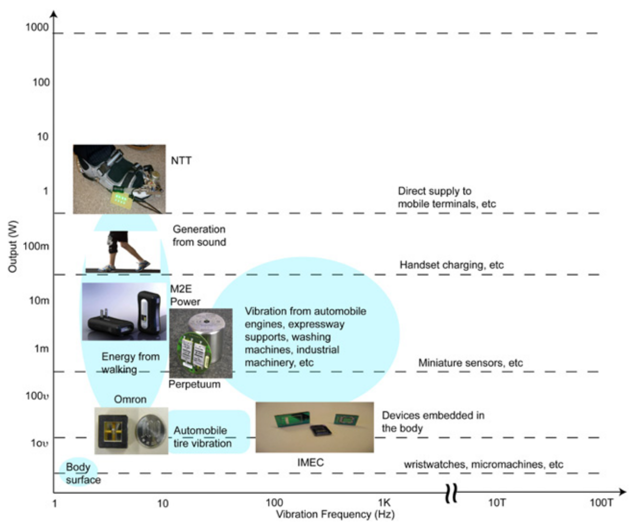

Figure 19. Power outputs along with possible operating frequencies from existing technologies for vibration-based energy harvesters manufactured by NTT, M2E Power, Omron Corporation, Perpetuum and IMEC [38].

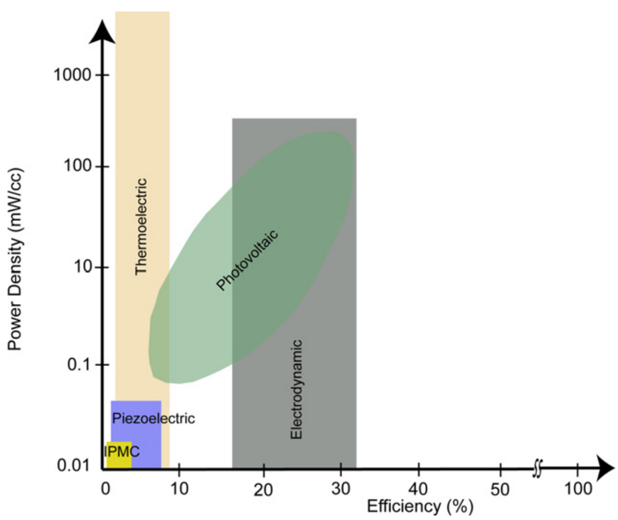

Figure 20. Power density comparison [65].

energy stored inside IPMC the efficiency could be increased. Although the research reported here focuses only on the transducer, there is still a need to address the efficiency losses in the energy harvesting circuit and storage devices.

5. Conclusion

An electromechanical transformer model was employed to study the effects of parameters in the mechanical and electrical domains on IPMC transduction. It was observed that the material's mechanoelectric output could be tailored by changing parameters like the material thickness, electrode–polymer interfacial area and electrode thickness.

Table 5. Comparison between IPMC and piezoelectric based energy harvesters.

Material	Efficiency (%)	Instantaneous power (per volume)	Frequency of application (Hz)
IPMC	<2	μW	<100
PZT [63]	5–7	mW	>100
PVDF [67]	3–4	μW	>100

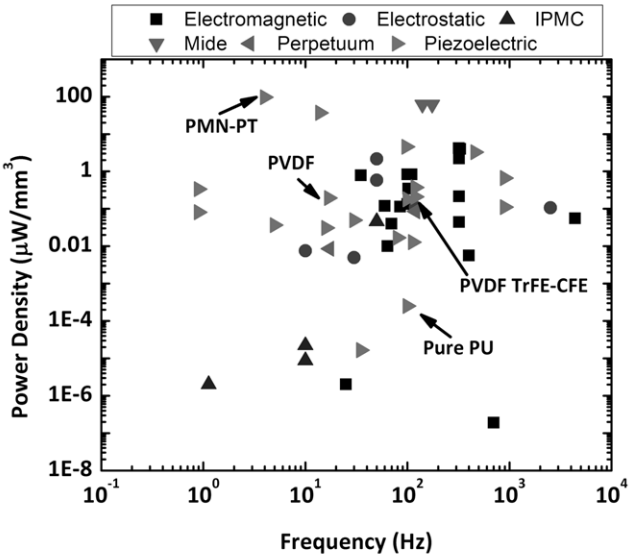

Figure 21. Power densities and operating frequencies of different vibration energy harvesters (data taken from [1, 83–104]).

The mechanoelectric output of the IPMC was highly dependent on the impedance of the samples. The electrodes in IPMC consist of metal particles dispersed in the polymer matrix. The density of metal particles is higher on the surface and reduces gradually towards the bulk of the material. The ions in the polymer matrix form the electric double layer and accumulate around the metal particles. The amount of charge accumulation in turn is dependent on the interfacial area. On the other hand, the flow of current in the electrode layer is affected by the conductivity through the thickness of the electrode.

An improvement in battery charging was achieved by reducing the surface or intermediate layer impedance. This could be achieved by increasing the capacitance, C, as

$$Z_C = \frac{1}{2\pi F_r C}, \tag{15}$$

where F_r is the frequency. From equation (15) it is evident that increasing the capacitance reduced the capacitive impedance (Z_C). The intermediate layer impedance could be reduced either by increasing the thickness of the electrode deposition or by dispersing more metal particles inside the polymer, as more particles lead to improvement in the polymer conductivity.

In the reported research it was also shown that IPMC is capable of harvesting energy from low-frequency vibration (<50 Hz). The power density of IPMC with platinum electrodes for tip excitation was measured to be around 45 μW cm^{-3}. Although IPMC shows a lower efficiency of around 2%, it could be argued that it is comparable to the current state of the art. The lower efficiency of IPMC could be due to elastic, dielectric, electrical and thermal energy losses. The stress–strain curve for IPMC obtained at room temperature depicts viscoelastic behavior. The viscoelastic nature of IPMC causes it to convert mechanical energy into heat energy on deformation. The mechanical losses in IPMC can be described in terms of loss and storage moduli. The energy dissipated can be described using the loss factor. The efficiency could also be increased by decreasing the dielectric losses as these losses cause a decrease in the permittivity of the material and hence the capacitance. In addition, there may be some thermoelastic losses due to vibration of the material. Further study is required in order to investigate these factors in detail. Additionally, in all energy harvesting systems, electric energy is consumed by the electronics and hence must in taken into consideration. The efficiency reported in this research does not take into account the losses associated with the energy harvesting circuits.

Further work is needed to study the effect of tailoring IPMC properties on its efficiency and frequency response. The transformer model could also be further investigated to incorporate the effects of diffusion and ion transport inside the IPMC. As IPMC is a composite, whose properties are dependent on its hydration, ionomer structure, metal particle distribution and electrode properties, it becomes very difficult to accurately determine material constants such as the diffusion coefficient, the dielectric constant and the individual layer impedances. Also, there is a need to study the effects of different material properties on ion transport inside IPMC.

Acknowledgment

This material is based upon work partially supported by the National Science Foundation under Grant No. #0713075.

References

[1] Tiwari R, Kim K J and Kim S-M 2008 Ionic polymer metal composite as energy harvester *Smart Struct. Syst.* **4** 549–63
[2] Anton S R and Sodano H A 2007 A review of power harvesting using piezoelectric materials *Smart Mater. Struct.* **16** R1–R21
[3] Lefeuvre E, Badel A, Richard C and Guyomar D 2007 Energy harvesting using piezoelectric materials: case of random vibrations *J. Electroceram.* **19** 349–55
[4] Bennett M D, Leo D J, Wilkes G L, Beyer F L and Pechar T W 2006 A model of charge transport and electromechanical transduction in ionic liquid swollen nafion membranes *Polymer* **47** 6782–96
[5] Kasyap A, Lim J, Johnson D, Horowitz S, Nishida T, Ngo K, Sheplak M and Cattafesta L 2002 Energy reclamation

from a vibrating piezoceramic composite beam *Proc. 9th Int. Cong. Sound Vib. (Orlando FL)* 271

[6] Ottman G K, Hofmann H F, Bhatt C A and Lesieutre G A 2002 Adaptive piezoelectric energy harvesting circuit for wireless, remote power supply *IEEE Trans. Power Electron.* **17** 1–8

[7] Hofmann H, Ottman G K and Lesieutre G A 2002 Optimized piezoelectric energy circuit using step-down converter in discontinuous conduction mode *IEEE Trans. Power Electron.* **18** 696–703

[8] Sodano H A, Inman D J and Park G 2004 A review of power harvesting from vibration using piezoelectric materials *Shock Vibr. Dig.* **36** 197–205

[9] Takenaka H, Torikai E, Kawami Y and Wakabayashi N 1982 *Int. J. Hydrog. Energy* **7** 397–403

[10] Millet P, Pineri M and Durand R 1989 *J. Appl. Electrochem.* **19** 162–6

[11] Millet P, Andolfatto F and Durand R 1995 *J. Appl. Electrochem.* **25** 233–9

[12] Bonomo C, Fortuna L, Giannone P and Graziani S 2004 A sensor actuator integrated system based on IPMC *Proc. Sensors* **1** 489–92

[13] Akle B J and Leo D J 2004 Electromechanical transduction in multilayer ionic transducers *Smart Mater. Struct.* **13** 1081

[14] Pak J J, Kim J, Oh S W, Son J H, Cho S H, Lee S-K, Park J-Y and Kim B 2004 Fabrication of ionic-polymer–metal-composite (IPMC) micro-pump using a commercial nafion *Proc. SPIE Smart Struct. Mater. Symp. EAPAD Conf.* **5385** 272–80

[15] Kim K J, Paquette J, Leo D and Farinholt K M 2006 Ionic polymer–metal composite for sensory applications *Encyclopedia of Sensors* ed C A Grimers and E C Dickey (Valencia, CA: American Scientific Press) chapter 15

[16] Bonomo C, Brunetto P, Fortuna L, Giannone P, Graziani S and Strazzeri S 2008 A Tactile sensor for biomedical applications based on IPMCs? *IEEE Sens. J.* **8** 1486–93

[17] Nemat-Nasser S 2002 Micromechanics of actuation of ionic polymer–metal composites *J. Appl. Phys.* **92** 2899–915

[18] Akle B J and Leo D J 2008 Single-walled carbon nanotubes ionic polymer electroactive hybrid transducers *J. Intell. Mater. Syst. Struct.* **19** 905–15

[19] Kothera C S 2002 Micro-manipulation and bandwidth characterization of ionic polymer actuators *MS Thesis* Virginia, Blacksburg

[20] Bonomo C, Negro C D, Fortuna L and Graziani S 2003 Characterization of IPMC strip sensorial properties: preliminary results *Proc. Int. Symp. Circuits Syst.* **4** IV-816–9

[21] Duncan A J, Leo D J and Long T E 2008 *Macromolecules* **41** 7765–75

[22] Kanno R, Kurata A, Hattori M, Tadokoro S, Takamori T and Oguro K 1994 Characteristics and modeling of ICPF actuator *Proc. Japan–USA Symp. on Flexible Automation (Tokyo)* 2, pp 691–8

[23] Asaka K, Oguro K, Nishimura Y, Mizuhata M and Takenaka H 1995 Bending of polyelectrolyte membrane platinum composites by electric stimuli i: response characteristics to various waveforms *Polym. J.* **27** 436–40

[24] Bar-Cohen Y (ed) 2001 *Electroactive Polymer (EAP) Actuators as Artificial Muscles—Reality, Potential and Challenges* PM98 SPIE Press pp 1–671

[25] Bao X, Bar-Cohen Y and Lih S-S 2002 Measurements and macro models of ionomeric polymer–metal composites (IPMC) *Proc. SPIE Smart Struct. Mater. Symp.* **4695** 220–7

[26] Kanno R, Tadokoro S, Takamori T and Hattori M 1996 Linear approximate dynamic model of icpf (ionic conducting polymer gel film) actuator *Proc. IEEE Int. Conf. on Robot. Autom.* pp 219–25

[27] Nemat-Nasser S 2008 Electro-chemomechanics of ionic polymer-metal composites *Handbook of Experimental Solid Mechanics* ed W Sharpe (Berlin: Springer-Verlag) ISBN 978-0-387-26883-5 187-201

[28] Madden J D W, Vandesteeg N A, Anquetil P A, Madden P G A, Takshi A, Pytel R Z, Lafontaine S R, Wieringa P A and Hunter I W 2004 *IEEE J. Oceanic Eng.* **29** 706

[29] EAMEX Corporation www.eamex.co.jp

[30] Colozza A 2007 *IEEE Spectr.* **44** 38

[31] Sewa S, Onishi K, Asaka K, Fujiwara N and Oguro K 1998 *Proc. IEEE Workshop Microelectromech Syst: Invest. Micro Struct. Sens. Actuators Mach. Syst.* **148**

[32] Oguro K, Fujiwara N, Asaka K, Onishi K and Sewa S 1999 *Proc. SPIE Smart Struct. Mater. Symp., EAPAD Conf.* **3669** 64

[33] Paquette J and Kim K J 2004 *IEEE J. Oceanic Eng.* **29** 729

[34] Bar-Cohen Y, Leary S, Yavrouian A, Oguro K, Tadokoro S, Harrison J, Smith J and Su J 2000 *Proc. SPIE Smart Struct. Mater. Symp. EAPAD Conf.* **3987** 140

[35] Smela E 2003 *Adv. Mater.* **15** 481

[36] Nemat-Nasser S and Li J 2000 Electromechanical response of ionic polymer metal composite *J. Appl. Phys.* **87** 3321–31

[37] Farinholt K and Leo D 2004 Modeling of electromechanical charge sensingin ionic polymer transducers *Mech. Mater.* **36** 421–33

[38] Weiland L M and Leo D J 2004 Electrostatic analysis of clusterresponse to electrical and mechanical loading in ionic polymers with cluster morphology *Smart Mater. Struct.* **13** 323–36

[39] De Gennes P G, Okumura K, Shahinpoor M and Kim K J 2000 Mechanoelectric effects in ionic gels *Europhys. Lett.* **50** 513–8

[40] Punning A 2007 Electromechanical characterization of ionic polymer metal composites sensing actuator *PhD Dissertation* University of Tartu, Estonia

[41] Martin B R 2005 Energy harvesting applications of ionic polymers *M S Thesis* Virginia Polytechnic Institute and State University

[42] Brufau-Penella J, Puig-Vidal M, Graziani S and Strazzeri S 2008 Characterization of the harvesting capabilities of an ionic polymer metalcomposite device *Smart Mater. Struct.* **17** 015009

[43] Aureli M, Lin W and Porfiri M 2009 On the capacitance-boost of ionic polymer metal composites due to electroless plating: theory and experiments *J. Appl. Phys.* **105** 104911

[44] Aureli M, Prince C, Porfiri M and Peterson S D 2010 Energy harvesting from base excitation of ionic polymer metal composites in fluid environments *Smart Mater. Struct.* **19** 015003

[45] Giacomello A and Porfiri M 2011 Underwater energy harvesting from aheavy flag hosting ionic polymer metal composites *J. Appl. Phys.* **109** 084903

[46] Tiwari R and Kwang K 2010 Disc-shaped ionic polymer metal composites for use in mechanoelectrical applications *Smart Mater. Struct.* **19** 065016

[47] Farinholt K M, Pedrazas N A, Schluneker D M, Burt D W and Farrar C R 2009 An energy harvesting comparison of piezoelectric and ionically conductive polymers *J. Intell. Mater. Syst. Struct.* **20** 633–42

[48] Newbury K and Leo D J 2002 Electromechanical modeling and characterization of ionic polymer benders *J. Intell. Mater. Syst. Struct.* **13** 51–60

[49] Konyo M, Konishi Y, Tadokoro S and Kishima T 2004 Development of velocity sensor using ionic polymer metal composites *Proc. SPIE Smart Struct. Mater. Symp. EAPAD Conf.* **5385** 394

[50] Kim K J, Paquette J, Leo D and Farinholt K M 2006 Ionic polymer-metal composite for sensory applications *Encyclopedia Sensors* 1–20
[51] Nemat-Nasser S and Thomas C W 2004 Chapter 6: ionic polymer–metal composites *Electroactive Polymer Actuators as Artificial Muscles: Reality, Potential and Challenges* 2nd edn, ed Y Bar-Cohen (Bellingham, WA: SPIE Publication)
[52] Sodano H A, Inman D J and Park G 2004 Generation and storage of electricity from power harvesting devices *J. Intell. Mater. Syst. Struct.* **16** 67–75
[53] Qiu J, Jiang H, Ji H and Zhu K 2009 Comparision between fourpiezoelectric energy harvesting circuits *Frontier Mech. Eng. China* **4** 153–9
[54] Oguro 2001 *Recipe-IPMC* ed Y Bar-Cohen http://ndeaa.jpl.nasa.gov/nasa-nde/lommas/eap/IPMCPrepProcedure.htm
[55] Shahinpoor M and Kwang K 2000 The effect of surface-electrode resistance on the performance of ionic-polymer metal composite artificialmuscles *Smart Mater. Struct.* **9** 543
[56] Chen Z, Tan X, Will A and Ziel C 2007 A dynamic model for ionic polymermetal composite sensors *Smart Mater. Struct.* **16** 1477–88
[57] Kim S J, Kim S-M, Kwang K and Kim Y H 2007 An electrode model forionic-polymer metal composites *Smart Mater. Struct.* **16** 2286
[58] Noh T-G, Tak Y, Nam J-D and Choi H 2002 Electrochemical characterization of polymer actuator with large interfacial area *Electrochim. Acta* **47** 2341–6
[59] Jung S, Song J, Kim G, Lee S and Mun M 2007 Effect of the electrode interface on the electric properties of artificial muscles *Proc. World Cong. Med. Phys. BioMed. Eng.* **14** 2973–6
[60] Punning A, Kruusmaa M and Aabloo A 2007 Surface resistance experiments with IPMC sensors and actuators *Sensors Actuators* A **133** 200–9
[61] Kim S J, Kim S-M, Kim K J and Kim Y H 2007 *Smart Mater. Struct.* **16** 2286–95
[62] Kim K J and Shahinpoor M 2002 *Polymer* **43** 797–802
[63] Sodano H A and Inman D J 2005 Comparison of piezoelectric energy harvesting devices for recharging batteries *J. Intell. Mater. Syst. Struct.* **16** 799–807
[64] Nikkei Electronics 2009 www.techon.nikkeibp.co.jp
[65] Harrop P 2009 Payback From Energy Harvesting IDTechEx www.greenspacetoday.com/green-guide/paybacks-energy-harvesting
[66] Charnegie D 2007 Frequency tuning concepts for piezoelectric cantileverbeams and plates for energy harvesting *M S Thesis* University of Pittsburg
[67] Goldfarb M and Jones L D 1999 On the efficiency of electric power generation with piezoelectric ceramics *J. Dyn. Syst. Meas. Control* **121** 566–71
[68] Tiwari R and Garcia E 2011 The state of understanding ionic polymer metal composite architecture: a review *Smart Mater. Struct.* **20** 083001
[69] Shahinpoor M and Kim K J 2001 *Smart Mater. Struct.* **10** 819–33
[70] Fujiwara N, Asaka K, Nishimura Y, Oguro K and Torikai E 2000 *Chem. Mater.* **12** 1750–4
[71] Kim D and Kim K J 2006 *J. Intell. Mater. Syst. Struct.* **17** 449–54
[72] Fang B-K, Ju M-S and Lin C-C K 2007 *Sensors Actuators* A **137** 321–9
[73] Palmre V, Brandell D, Maeorg U, Torop J, Volobujeva O, Punning A, Johanso U, Kruusmaa M and Aabloo A 2009 *Smart Mater. Struct.* **18** 095028
[74] Guyomar D and Lallart M 2011 *Micromachines* **2** 274–94
[75] Schlichting A, Tiwari R and Garcia E 2012 *J. Intell. Mater. Syst. Struct.* **23** 1921–35
[76] Huang S C and Lin K-A 2012 *Smart Mater. Struct.* **21** 085014
[77] Shafer M W, Bryant M and Garcia E 2012 *Smart Mater. Struct.* **21** 085008
[78] Najem J, Sarles S A, Akle B and Leo D J 2012 *Smart Mater. Struct.* **21** 094026
[79] Park I-S, Tiwari R and Kim K J 2009 *Adv. Sci. Technol.* **61** 59–64
[80] Tiwari R and Kim K J *Ionic Interactions in Natural and Synthetic Macromolecules* ed A Ciferri and A Perico (Hoboken, NJ: Wiley)
[81] Lee G-Y, Choi J-O, Kim M and Ahn S-H 2011 *Smart Mater. Struct.* **20** 105026
[82] Gutta S, Lee J S, Trabia M B and Yim W 2012 *Smart Mater. Struct.* **18** 115023
[83] Tiwari R 2012 *Int. J. Smart Nano Mater.* **3** 275–95
[84] Tiwari R and Kim K J 2010 *Appl. Phys. Lett.* **97** 244104
[85] Chiba S, Waki M, Kornbluh R and Pelrine R 2011 *Smart Mater. Struct.* **20** 124006
[86] Liu Y, Liu L, Zhang Z, Jiao Y, Sun S and Leng J 2010 *Europhys. Lett.* **90** 36004
[87] Pelrine R, Kornbluh R, Eckerle J, Jeuck P, Oh S, Pei Q and Stanford S 2001 *Proc. SPIE* **4329** 148–56
[88] Kornbluh R D http://spie.org/documents/Newsroom/Imported/003749/003749_10.pdf
[89] http://dr.berkeley.edu/pdfs_to_post/SCAVENGING_MICRO_ENERGY_FROM_THE_ENVIRONMENT_TO_PROVIDE_BATTERY_FREE_WIRELESS_SENSOR_NETS.pdf
[90] Kim H, Bedekar V, Islam R, Lee W H, Leo D and Priya S 2008 *IEEE Ultrason. Freq. Ferroelectr. Control* **55** 1900–5
[91] Cottiner P-J, Guyomar D, Guiffard B, Putson C and Lebrun L 2010 *IEEE Trans. Ultrason. Ferroelecr. Freq. Control* **57** 774–84
[92] Park J-h 2010 Development of MEMS piezoelectric energy harvesters *PhD Dissertation* Auburn University
[93] Cottiner P-J, Guyomar D and Lallart M 2010 *Sensors Actuators* A **172** 497–503
[94] Sterken T, Fiorini P, Baert K, Puers R and Borghs G 2003 *Int. Conf. Solid State Sensors Actuators Microsyst. Transducers* 1291–4
[95] Miao Mitcheson P D, Holmes A S, Yeatman E M, Green T C and Stark B H 2006 *Microsyst. Technol.* **12** 1079–83
[96] Despesse G, Chaillout J J, Jager T, Cardot F and Hoogerwerf A 2007 *Int. Conf. Solid State Sensors Actuators Microsyst. Transducers* 895–8
[97] Glynne-Jones P, Beeby S P, James E P and White N M 2001 *Int. Conf. Solid State Sensors Actuators Microsyst. Transducers* 46–9
[98] Marzencki M, Ammar Y and Basrour S 2007 *Int. Conf. Solid State Sensors Actuators Microsyst. Transducers* **887–890**
[99] Renaud M, Sterken T, Schmitz A, Fiorini P, Van Hoof C and Puers R 2007 *Int. Conf. Solid–State Sensors, Actuators Microsyst., Transduc.* 891–4
[100] Elfrink R, Kamel T M, Goedbloed M, Matova S, Hohlfeld D and van Schaijk R 2008 *Proc. Power MEMS Workshop (Sendai, Nov.)* pp 249–52
[101] Kulkarni S, Koukharenko E, Tudor J, Beeby S, O'Donnell T and Roy S 2007 *Int. Conf. Solid State Sensors Actuators Microsyst. Transducers* 879–82
[102] Torah R N, Beeby S P, Tudor M J, O'Donnell T and Roy S 2006 *Proc 6th Int. Workshop Micro Nanotechnol Power Generation Energy Conversion Application (Berkeley, CA)* pp 181–4
[103] Glynne-Jones P, Tudor M J, Beeby S P and White N M 2004 *Sensors Actuators* A **110** 344–9
[104] Lee J M H, Yuen S C, Li W J and Leong P H W 2003 *Proc. Int Symp. Circuits Syst.* 4, Bangkok pp 876–9